Bulk Quantum Computation with Nuclear Magnetic Resonance: Theory and Experiment

Isaac L. Chuang[1*], Neil Gershenfeld[2], Mark G. Kubinec[3], and Debbie W. Leung[4]

[1] *Los Alamos National Laboratory, Theoretical Astrophysics T-6*
Mail Stop B288, Los Alamos, NM 87545

[2] *Physics and Media Group, MIT Media Lab, Cambridge, MA 02139*

[3] *College of Chemistry, D7 Latimer Hall,*
University of California Berkeley, Berkley, CA 94720-1460

[4] *ERATO Quantum Fluctuation Project,*
Stanford University, Ginzton Laboratory, Stanford, CA 94305

(October 6, 1997)

We show that quantum computation is possible with mixed states instead of pure states as inputs. This is performed by embedding within the mixed state a subspace that transforms like a pure state and that can be identified by labeling it based on logical (spin), temporal, or spatial degrees of freedom. This permits quantum computation to be realized with bulk ensembles far from the ground state. Experimental results are presented for quantum gates and circuits implemented with liquid nuclear magnetic resonance techniques and verified by quantum state tomography.

I. INTRODUCTION

Quantum computation is a wonderful theoretical invention that presents a profound experimental challenge. The difficulty in building a quantum computer is to find a system that has the nonlinear interactions that are required for computation [1], and that simultaneously can be influenced externally in order to control it but that does not couple to the environment so strongly that the quantum coherence is rapidly lost [2,3]. Even if this is possible with a few quantum degrees of freedom, the experimental effort to scale up to larger systems can be daunting.

To realize a quantum computer it is necessary to demonstrate that macroscopic measurements and manipulations can be used to act on microscopic quantum degrees of freedom, and that these can be used to accomplish four tasks: (1) prepare the system in a fiducial initial state (a pure state such as the ground state), (2) perform arbitrary single qubit operations, (3) apply universal two-qubit functions (such as a controlled–NOT [4]), and (4) implement projective measurement to read out the computational results.

Each of these tasks must be accomplished within the coherence time of the system. This can be extremely diffi-cult because of the ubiquitous nature of interactions leading to decoherence. Since just a small amount of decoherence can disrupt a quantum computation [3,5], quantum decoherence is the largest obstacle in the road to practical quantum computing machines [2,6]. Many candidate physical systems have been suggested that might provide experimental access while preserving quantum coherence, including spin chains, polymers, and quantum dots [7–9], isolated magnetic spins [10], trapped ions [11], optical photons [12,13], and cavity quantum-electrodynamics [14,15].

While all of these systems show some promise, nuclear magnetic resonance (NMR) [8,10,16] is particularly attractive because of the extremely long coherence times (up to thousands of seconds) due to the natural isolation of the nucleus. NMR is also attractive experimentally because of the complexity of operations which can be accomplished using modern spectrometers [17]. However, NMR is a bulk phenomenon – an aggregate signal from many individual molecules is necessary for practical observation [18] – and unfortunately, such a system does not fulfill requirements (1) and (4) above. Practically obtainable initial states are thermal statistical mixtures, not pure states, and the computational results from individual members of the ensemble are made inaccessible by the averaging. These two issues have kept NMR from being useful for quantum computation.

However, we have recently shown that NMR can in fact be used to perform quantum computations, using ordinary liquids at room temperature and standard pressure, with standard commercial instrumentation [19]. These results were made possible by using a new procedure to take advantage of the structure present in thermal equilibrium to introduce into the system's large density matrix a perturbation that acts exactly like a much smaller dimensional *effective pure state*. Another new step which we described was how to modify the computational procedure to provide a *deterministic* result that does not average away in an ensemble measurement.

In this paper we extend our previous theoretical results

---

*Electronic address: ike@lanl.gov

to present a general framework for understanding how to perform quantum computation using mixed state inputs instead of pure states. In Section II, we show how our techniques to create effective pure states can be understood using the notion of *state labeling*: attaching logical, spatial, or temporal labels to the quantum state in such a way that a subspace within the mixed state can be identified and utilized for quantum computation. Practically speaking, these results herald the introduction of *bulk quantum computers*, which work using ensembles of quantum systems rather than with single systems.

We present in Section III experimental results demonstrating progress towards realization of bulk quantum computers using NMR. We show a controlled-NOT gate implemented using state labeling on a simple two-spin system, and have developed techniques for performing quantum state tomography to test it. We have also succeeded in cascading controlled-NOT gates to create a circuit to perform a permutation operation, and in using this to create an effective pure state which is input to a quantum circuit to create an Einstein-Podolsky-Rosen entangled state [20].

II. STATE LABELING TO CREATE EFFECTIVE PURE STATES

A bulk quantum computer is an ensemble of many small quantum computers, all of which work independently in parallel, but are subject to two restrictions. First, the initial state of each machine is determined at random, and second, the only measurement result accessible is an ensemble average of the computers' registers. These limitations are problematic for quantum computation, which usually requires a pure state input, and measurement of each quantum computer's results. The latter limitation can be dealt with by using deterministic quantum algorithms, as we have previously described [19]. The former problem can be resolved by creating effective pure states, using a technique we describe in this section.

An ensemble of identical quantum systems need not have all of its members be in identical pure quantum states in order for the ensemble to behave like a pure quantum state. For example, even if only a fraction of all the systems are in their ground states, then as long as the remaining systems are arranged such that their signals cancel out, only the small fraction will be visible, and the ensemble will appear to be pure. Alternatively, if we can label a select fraction of states, and then *cause* the remainder to average away, then we will also obtain an effective pure state. We mathematically define both the notion of an effective pure state, and techniques for creating it below.

A. Effective Pure States

An effective pure state is a state that behaves for all computational purposes as a pure state. In general, quantum logic operations are unitary operations. However, if one considers initial state preparation and measurement processes as part of the calculation, the combined computation process is a general trace-preserving quantum operation $\mathcal{C}(\hat{\rho}) = \sum_k \hat{A}_k \hat{\rho} \hat{A}_k^\dagger$, where $\hat{A}_k$ are linear operators satisfying the condition $\sum_k \hat{A}_k^\dagger \hat{A}_k = \hat{I}$ [21,22]. The density matrix $\hat{\rho}_\epsilon$ is an effective pure state for a computation $\mathcal{C}$ corresponding to an actual pure state $|\psi\rangle\langle\psi|$, if there exists a transformation from $\mathcal{C}$ to another computation $\mathcal{C}'$ such that the computation $\mathcal{C}'$ with input $\hat{\rho}_\epsilon$ and the computation $\mathcal{C}$ with input $|\psi\rangle\langle\psi|$ give results proportional to each other for a set of non-trivial (i.e., computationally meaningful) observables $\hat{O}_i$. In other words, $\hat{\rho}_\epsilon$ is an effective pure state for $\mathcal{C}$ corresponding to $|\psi\rangle\langle\psi|$ if

$$\mathrm{Tr}(\mathcal{C}'(\hat{\rho}_\epsilon)\hat{O}_i) = \alpha\,\mathrm{Tr}(\mathcal{C}|\psi\rangle\langle\psi|)\hat{O}_i)\,, \tag{1}$$

for some fixed known constant α.

Let us see what this operational definition means. Without loss of generality, we may take a quantum computation to be a unitary transform which acts on a ground state $|\phi_0\rangle\langle\phi_0|$ as input. In theory, the result from any quantum computation can be arranged to be the state of a single qubit in the computational basis. Subsequent iterations of such "standardized quantum computations" can give additional higher order qubits of the answer, one at a time, in time manifestly linear in the total number of qubits N. Without loss of generality, we may therefore let the measurement operator for the final outcome be just the Pauli matrix σ_z, acting in the Hilbert space of the one readout qubit. The important observation is that for a standardized quantum computation $\mathcal{C}$, and for any α,

$$\hat{\rho}_\epsilon = \frac{1-\alpha}{2^N}\hat{I} + \alpha|\psi\rangle\langle\psi| \tag{2}$$

will be an effective pure state for $\mathcal{C}$, since

$$\begin{aligned}
\mathrm{Tr}\left(\mathcal{C}(\hat{\rho}_\epsilon)\sigma_z\right) &= \mathrm{Tr}\left[\sum_k \hat{A}_k \hat{\rho}_\epsilon \hat{A}_k^\dagger \sigma_z\right] \\
&= \sum_k \mathrm{Tr}\left[\left(\frac{1-\alpha}{2^N}\hat{A}_k\hat{A}_k^\dagger + \alpha\hat{A}_k|\psi\rangle\langle\psi|\hat{A}_k^\dagger\right)\sigma_z\right] \\
&= \alpha\,\mathrm{Tr}\left[\mathcal{C}(|\psi\rangle\langle\psi|)\sigma_z\right]\,, \tag{3}
\end{aligned}$$

due to the fact that σ_z is traceless, and using the cyclic property of the trace, the trace preserving condition $\sum_k \hat{A}_k^\dagger \hat{A}_k = \hat{I}$, and the unitarity constraint $\mathcal{C}(\hat{I}) = \hat{I}$. The same result is obtained for any measurement observable $\hat{O}_i$ which is traceless.

2

For standardized quantum computations, only deviations of the density matrix $\hat{\rho}$ from the identity are relevant. We define the *deviation density matrix* $\hat{\rho}_\Delta$ as

$$\hat{\rho}_\Delta = \hat{\rho} - \frac{\hat{I}}{d}, \tag{4}$$

where $d = 2^N/\mathrm{Tr}(\hat{\rho})$. For the remainder of this paper unless otherwise noted we shall limit our attention to deviation density matrices. Note that $\hat{\rho}_\Delta$ transforms identically to $\hat{\rho}$ under unitary quantum operations, since $\hat{U}\hat{\rho}_\Delta\hat{U}^\dagger = \hat{U}\hat{\rho}\hat{U}^\dagger$. In general, for non-unitary operations, we have that $\mathcal{E}(\hat{\rho}) = \sum_k \hat{A}_k\hat{\rho}\hat{A}_k^\dagger = \mathcal{E}(\hat{\rho}_\Delta) - \mathcal{E}(\hat{I})/d$, so aside from a factor which is constant with respect to changes in $\hat{\rho}_\Delta$, we find that the dynamical behavior of $\hat{\rho}_\Delta$ fully describes the behavior of the system.

Because $\mathrm{Tr}(\hat{\rho}_\Delta) = 0$ for any $\hat{\rho}$, $\hat{\rho}_\Delta$ will be an effective pure state for any standardized $\mathcal{C}$ if its eigenvalues are $\alpha, -\delta, -\delta, -\delta, \ldots$, where $\delta = \alpha/(2^N - 1)$. This class of effective pure states is universal for all standardized computations and requires no modification of the computation procedure. It can be interpreted as describing a system which is highly uniform – a "choir" of energy eigenstates which are all equally populated – except for one "soloist," an eigenstate with a different population. This picture is analogous to the existence of holes in a semiconductor. The system behaves like a pure state because only the signal of the soloist is measurable; the signal from any choir state is canceled by another state with the same population and will not be observed. This is different from a real pure state in that many underlying degrees of freedom can contribute to the effective degrees of freedom of $\hat{\rho}_\Delta$. Having established a definition for effective pure states, we turn next to describe how they can be created.

B. State Labeling

Given an arbitrary initial state $\hat{\rho}$, our goal is to produce from it an effective pure state to serve as input into a standardized computation $\mathcal{C}$. How can this be done?

One way to do it is to use extra spins as label states, and to prepend $\mathcal{C}$ with an initial preparation step $\mathcal{P}$ and append it with a readout preparation step $\mathcal{R}$, such that

$$\mathcal{C}'(\hat{\rho}) = \mathcal{R}\left[(\mathcal{I}_{label} \otimes \mathcal{C})\left[\mathcal{P}(\hat{\rho})\right]\right] = \alpha\mathcal{C}(|\phi_0\rangle\langle\phi_0|). \tag{5}$$

$\mathcal{C}'$, $\mathcal{R}$, and $\mathcal{P}$ denote general quantum operations. The purpose of $\mathcal{P}$ is to modify $\hat{\rho}$ by pushing some of its randomness into a label state. In particular, we may choose $\mathcal{P}$ such that

$$\mathcal{P}(\hat{\rho}) = \sum_k P_k\hat{\rho}P_k^\dagger = \sum_k |k\rangle\langle k| \otimes \hat{\rho}_k, \tag{6}$$

where, say, $\hat{\rho}_0 = \alpha|\phi_0\rangle\langle\phi_0|$ is an effective pure state and the remaining $\hat{\rho}_k$ are undesired "garbage" states for $k \geq$

1. The $|k\rangle\langle k|$ are the eigenfunctions of the label degrees of freedom, with the $|0\rangle\langle 0|$ state identifying the effective pure state. The computation $\mathcal{I}_{label} \otimes \mathcal{C}$ is arranged to operate only on the Hilbert space of $\hat{\rho}_k$ and to leave the label state alone (experimentally, for spins this can be accomplished using standard refocusing and decoupling techniques [17]). For readout preparation, $\mathcal{R}$ is chosen to be the projection operation

$$\mathcal{R}(\hat{\rho}) = \left[|0\rangle\langle 0| \otimes \hat{I}\right] \hat{\rho} \left[|0\rangle\langle 0| \otimes \hat{I}\right] \tag{7}$$

where the signals in the other label states will be arranged to cancel out (how this can be implemented is described in the next section), so that for the overall computation we have

$$\mathcal{C}'(\hat{\rho}) = \sum_k \mathcal{R}(|k\rangle\langle k| \otimes \mathcal{C}(\hat{\rho}_k)) \tag{8}$$

$$= |0\rangle\langle 0| \otimes \alpha\mathcal{C}(|\phi_0\rangle\langle\phi_0|). \tag{9}$$

When conditioned upon the state of the label spins, the state of the remaining part of the Hilbert space is effectively pure, and a computation performed on this space can be selectively retrieved.

This technique is an example of *logical labeling*, where the label k is stored in a logical state of qubits embedded within the Hilbert space of the system. The most general application of state labeling may be written as

$$\mathcal{C}'(\hat{\rho}) = \sum_{j,k} \hat{R}_j \left[\mathcal{C}(\hat{P}_k\hat{\rho}\hat{P}_k^\dagger)\right] \hat{R}_j^\dagger, \tag{10}$$

where we have simply written out $\mathcal{P}$ and $\mathcal{R}$ as general quantum operations in the operator sum representation [21,22]. Such operations can be non-unitary; an obvious example is

$$\mathcal{C}'(\hat{\rho}) = \mathcal{C}\left(\sum_k \hat{P}_k\hat{\rho}\hat{P}_k^\dagger\right) = \mathcal{C}(\tilde{\rho}), \tag{11}$$

where $\mathcal{P}$ describes the effect of physical cooling or some sort of polarization transfer mechanism. This general approach to state labeling has found previous application in NMR interferometry in measuring the Aharonov-Anadan quantum phase [23], and in embedding spinors into multiple level spin systems [24].

Effective pure states have been created by Cory *et. al* [25] using an alternative technique that applies different unitary operations $\hat{P}_k$ as a function of a spatial degree of freedom k. This is experimentally implemented using gradient RF pulses, which rotate spins by an amount proportional to the location of the molecule in the physical apparatus (a useful technique for quenching magnetization). The operations are arranged such that the sum $\tilde{\rho}$ is an effective pure state. This is an example of *spatial labeling*.

Another way to simulate physical cooling to produce effective pure states is given by Knill [26]. A number of time-sequential unitary operations $\hat{P}_k$ are performed, chosen so that once again the sum $\bar{\hat{\rho}}$ is an effective pure state (an example is given is Section III G). Because the label k appears in the time index of the experiment this is an example of *temporal labeling*. The crucial point in this technique is to show that the number of $\hat{P}_k$ required is polynomial in the number of bits N.

State labeling is not just a way to create effective pure states; it also describes how to construct *robust* quantum computation procedures. Eq. (10) can be understood as a transformation from a given quantum computation $\mathcal{C}$ (which nominally operates on pure state inputs) into another one, $\mathcal{C}'$, which is robust in the sense that it can operate on a class of mixed state inputs. This notion of robust quantum computation significantly expands the physical systems available for quantum computation. We turn now to state labeling for the important experimental case of thermal states.

C. Labeling Thermal States

A convenient class of initial states arises from ensembles of quantum systems at high temperature. For example, the relevant case for conventional NMR is an N-spin system in a strong magnetic field at room temperature. In the energy eigenbasis, the density matrix $\hat{\rho}$ for the thermal equilibrium state is

$$\hat{\rho} = \frac{e^{-\beta\hat{\mathcal{H}}}}{\mathcal{Z}}, \tag{12}$$

where $\hat{\mathcal{H}}$ is the system Hamiltonian, $\beta = 1/k_B T$ is the inverse temperature, and $\mathcal{Z} = \sum_n \exp(-\beta E_n)$ is the partition function normalization factor (which gives $\mathrm{Tr}(\hat{\rho}) = 1$). If the N spins have nearly degenerate energies and weak couplings, then for evaluating populations $\hat{\mathcal{H}} \approx \sum_{k=0}^{N-1} \omega_k \sigma_z^{(k)}$ (measuring energy in angular units), where the superscript of the σ matrix is the spin label, and $\omega_k \approx \omega$ for all k. For $\omega \ll k_B T$, the deviation density matrix $\hat{\rho}_\Delta$ is well approximated as

$$\hat{\rho}_\Delta = \frac{-1}{2^N}\beta\hat{\mathcal{H}} \quad . \tag{13}$$

The preparation of an effective pure state from this thermal initial condition will be shown below, first for a three spin example and then for an arbitrary number of spins.

The relative population differences in an $N = 3$ system are

$$\begin{array}{cccccccc} \downarrow\downarrow\downarrow & \downarrow\downarrow\uparrow & \downarrow\uparrow\downarrow & \downarrow\uparrow\uparrow & \uparrow\downarrow\downarrow & \uparrow\downarrow\uparrow & \uparrow\uparrow\downarrow & \uparrow\uparrow\uparrow \\ 6 & 4 & 4 & 2 & 4 & 2 & 2 & 0 \end{array} \quad . \tag{14}$$

These populations may be pictured as shown in the energy level diagrams of Fig. 1. In contrast, a pure quantum state would have only one of the states populated. For example,

$$\begin{array}{cccc} \downarrow\downarrow & \downarrow\uparrow & \uparrow\downarrow & \uparrow\uparrow \\ 1 & 0 & 0 & 0 \end{array} \tag{15}$$

is a pure state of two qubits. This is different from a thermal state, which has populations in states other than the ground state. These extraneous populations generate signals which conflict with those from the desired one, destroying the computational output.
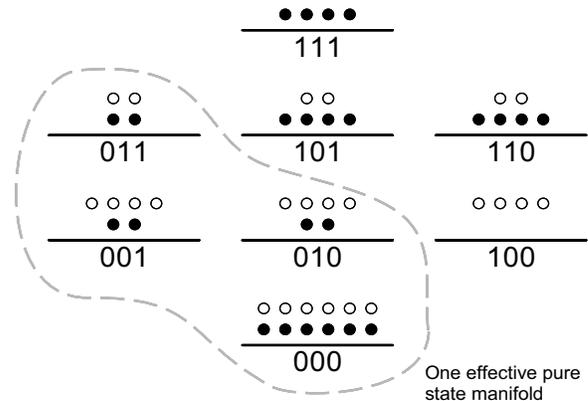
FIG. 1. Energy levels and populations of a three spin system. The initial thermal distribution is shown by the empty circles, and the populations of the "purified" state with effectively pure states are shown with filled circles.

However, if we had the population distribution

$$\begin{array}{cccc} \downarrow\downarrow & \downarrow\uparrow & \uparrow\downarrow & \uparrow\uparrow \\ 6 & 2 & 2 & 2 \end{array} \quad , \tag{16}$$

then we would have an effective pure state of two-qubits, because the net signal from such an ensemble is that generated by the *excess deviation* $(6 - 2 = 4)$ from the even background population (2). Such a population distribution may be constructed from Eq. (14) by using unitary operators (to be described below) to swap populations between different energy eigenstates to get

$$\begin{array}{cccccccc} \downarrow\downarrow\downarrow & \downarrow\downarrow\uparrow & \downarrow\uparrow\downarrow & \downarrow\uparrow\uparrow & \uparrow\downarrow\downarrow & \uparrow\downarrow\uparrow & \uparrow\uparrow\downarrow & \uparrow\uparrow\uparrow \\ 6 & 2 & 2 & 2 & 0 & 4 & 4 & 4 \end{array} \quad . \tag{17}$$

In this state, the first four eigenstates form a manifold which will act like a pure two qubit state, and the last four form another separate manifold which acts like another independent two qubit state. The first spin (the most significant qubit) determines which manifold we are in, and serves as a label which distinguishes the two possibilities. This label spin can be used to gate the output so that only one manifold or the other generates an output signal, so that no interference occurs between the two.

A general algorithm for creating an effective pure state from a thermal state, using logical labeling, is as follows.

The occurrence of each eigenvalue of the diagonal matrix Eq. (13) is given by a binomial distribution, with a maximum at $N!/[(N/2)!]^2$ zeros associated with states with an equal number of up and down spins. These can be chosen to be the "choir" (uniform background) states. The ground state, which is maximally populated, can then be selected to be the soloist. To see how the zeros can be moved into a pure state block in the density matrix, Eq. (13) can be written (for spin 1/2) as

$$\hat{\rho}_\Delta = \sum_{m_1=-1/2}^{1/2} \cdots \sum_{m_N=-1/2}^{1/2} (m_1 + m_2 + \cdots + m_N) \quad (18)$$
$$|m_1 m_n \ldots m_N\rangle\langle m_1 m_2 \ldots m_N| \quad .$$

The action of operators can be understood by their influence on the expansion coefficient. For six spins the coefficient starts out as

$$(m_1 + m_2 + m_3 + m_4 + m_5 + m_6) \quad . \quad (19)$$

If a controlled-NOT operation is performed by spin 1 on spin 4 ($CN_{1\to 4}$), the result is

$$(m_1 + m_2 + m_3 + 2m_1 m_4 + m_5 + m_6) \quad (20)$$
$$= (m_1(1 + 2m_4) + m_2 + m_3 + m_5 + m_6) \quad .$$

This means that if $m_1 = +1/2$ then m_4 is not changed, and if $m_1 = -1/2$ then m_4 changes sign. Following this by $CN_{2\to 5}$ and $CN_{3\to 6}$ (Fig. 2) gives a coefficient

$$m_1(1 + 2m_4) + m_2(1 + 2m_5) + m_3(1 + 2m_6) \quad . \quad (21)$$

This has a very natural interpretation. When $m_4 = -1/2$ the first term is equal to zero independent of the value of m_1. Similarly, when m_5 and $m_6 = -1/2$ the remaining terms vanish independent of m_2 and m_3. Therefore when spins 4-6 are down the coefficient is zero independent of the value of spins 1-3. This construction moves the chorus of spins 1-3 into a block labelled by the state of spins 4-6.
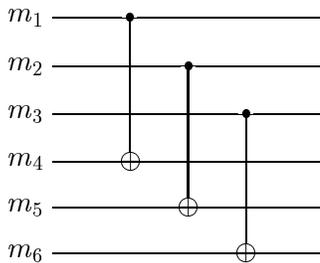
FIG. 2. Network of CNOT's to move zeros for 3 pure qubits $m_{1,2,3}$ conditioned on 3 ancilla $m_{4,5,6}$.

The final step in creating an effective pure state is to move the "soloist" into place. After the above algorithm, the state with the maximum population – the soloist – is in the state of all spins down, $|2^N - 1\rangle$. If we can perform the unitary transformation $\hat{U}_{add}|k\rangle = |k + 1 \mod 2^N\rangle$, then the chorus will shift downward, and the soloist will move from $|2^N - 1\rangle \to |0\rangle$. Thus, the first block of the density matrix will obtain the form $\text{diag}(\alpha, -\delta, -\delta, \ldots)$ which is our desired effective pure state.

The modular addition transform $\hat{U}_{add}$ can be implemented in three steps. Define $\omega \equiv \exp(2\pi i/2^N)$. First, perform the unitary Fourier transform $\hat{U}_{ft}$, then rotate the individual phase of the qth qubit around the $\hat{z}$ axis by ω^{2^q}, for all $0 \le q < N$, then perform the inverse unitary Fourier transform $\hat{U}_{ft}^\dagger$. Denote the rotation operation by $\hat{\theta}$. Then $\hat{U}_{ft}^\dagger \hat{\theta} \hat{U}_{ft} = \hat{U}_{add}$, proven as follows. First note that $\hat{\theta}$ performs the transform

$$\hat{\theta} = \sum_{l=0}^{2^N-1} \omega^l |l\rangle\langle l| , \quad (22)$$

as can be seen by expanding l in binary. Next, we calculate straightforwardly

$$\hat{U}_{ft}^\dagger \hat{\theta} \hat{U}_{ft} = \left[\frac{1}{\sqrt{2^N}} \sum_{p,k} \omega^{-pk} |p\rangle\langle k| \right] \cdot \left[\sum_l \omega^l |l\rangle\langle l| \right]$$
$$\cdot \left[\frac{1}{\sqrt{2^N}} \sum_{p',k'} \omega^{p'k'} |p'\rangle\langle k'| \right] \quad (23)$$

$$= \frac{1}{2^N} \sum_{p,k,k'} \omega^{k(-p+1+k')} |p\rangle\langle k'| \quad (24)$$

$$= \sum_{p,k'} |p\rangle\langle k'| \delta(p - 1 - k') \quad (25)$$

$$= \sum_p |p + 1 \mod 2^N\rangle\langle p| , \quad (26)$$

which is $\hat{U}_{add}$, as desired. Because $\hat{U}_{ft}$ can be implemented in $\mathcal{O}(N)$ steps [27], and since $\hat{\theta}$ is composed from single qubit operations, this circuit can be performed in $\mathcal{O}(N)$ time, for finite required precision, with a precision-dependent prefactor. In general, we note that many simple permutations (in particular, all cyclic permutations) can be implemented as easily as single bit operations in the Fourier space.

Our algorithm to create a logically labeled effective pure state from a high temperature deviation density matrix thus has two parts for the preparation step. The extension of the first part to N spins is straightforward, requiring $N/2$ steps to move the zeros for $N/2$ pure qubits starting from N thermal spins. Half of the N spins are used in the effective pure state, and the other half serve as ancilla for the purification procedure. This works for any N, but is not optimal. Asymptotically there are approximately $N - O(\log_2 N)$ zeros in the thermal density matrix, therefore a more efficient packing can approach N qubits from N spins.

The final readout preparation step, Eq. (7), is implemented in the following manner. Consider taking a measurement of σ_z on a state $\hat{\rho} = \sum_k |k\rangle\langle k| \otimes \hat{\rho}_k$. Such states result from performing a computation on logically labeled effective pure states such as those described above. Only the signal from one manifold, for example, $k = 0$, is desired; the remainder is unwanted "garbage." To subtract the signal due to the garbage states, results can be read out in two steps. First, a readout is performed with no transform (with a readout operator which is just the identity)

$$R_1 = \frac{1}{2}(\hat{I} \otimes \hat{I}) \quad . \tag{27}$$

The computation is then repeated and read out with the operator

$$R_2 = \frac{1}{2}\left[|0\rangle\langle 0| \otimes \hat{I} + \sum_{k \geq 1} |k\rangle\langle k| \otimes \sigma_x\right] \quad . \tag{28}$$

This operation can be accomplished using controlled-NOT logic gates. Summing the results of these two operations, one obtains the state

$$\hat{\rho}' = |0\rangle\langle 0| \otimes \hat{\rho}_0 + \frac{1}{2}\sum_{k \geq 1} |k\rangle\langle k| \otimes [\hat{\rho}_k + \sigma_x \hat{\rho}_k \sigma_x] \quad . \tag{29}$$

The measurement signal $\mathrm{Tr}(\hat{\rho}'\sigma_z)$ contains contributions only from $\hat{\rho}_0$, because for $k \geq 1$, $\hat{\rho}_k$ and $\sigma_x\hat{\rho}_k\sigma_x$ cancel out each other due to anticommutivity with σ_z. This provides the desired result from the computation, and completes our description of how to perform logical labeling to prepare effective pure states from a thermal state for arbitrary standardized quantum computations.

D. Scaling

Not all effective pure states are created equal. Even though they might be identical computationally, there can be enormous differences in the scaling of the signal strength, operator time, and size of fluctuations as the number of qubits is increased. This issue is particularly of concern when performing spatial or temporal labeling [28].

For state labeling a serious handicap is the decrease in signal strength as the number of bits N is increased. Most NMR experiments detect the transverse magnetization of one of the species

$$M_{xA} = n\langle\mu_{xA}\rangle = n\gamma_A\hbar\,\mathrm{Tr}(\hat{\rho}\sigma_{xA}) \quad , \tag{30}$$

where n is the density of the detected spin A with gyromagnetic ratio γ_A and σ_{xA} is the Pauli matrix for its x component (a quadrature measurement gives both the in-phase component μ_{xA} and the out-of-phase component

μ_{yA}). Any density matrix can be expanded in products of angular momentum operators, and because of their orthogonality property the only term that will contribute to this measurement is the one associated with σ_{xA}. For readout, the result of a computation is transferred to this term. Because a unitary computation can not change the eigenvalue spectrum of $\hat{\rho}_\Delta$, the largest signal possible is given by the largest eigenvalue of $\hat{\rho}_\Delta$. For the thermal equilibrium deviation density matrix this is given by the state with all the spins aligned with the field B (ignoring the exchange interactions which are much smaller than Zeeman energies in typical fields). Since in thermal equilibrium $\hat{\rho}_\Delta = \beta\hat{\mathcal{H}}/2^N$, for a spin $1/2$ system with gyromagnetic ratio γ_B the value of this eigenvalue is then

$$\frac{1}{2^N}\frac{\gamma_B\hbar B}{kT}\frac{N}{2} \quad . \tag{31}$$

Therefore the maximum readout magnetization is

$$M_{xA} = n\gamma_A\hbar\left[\frac{1}{2^N}\frac{\gamma_B\hbar B}{kT}\frac{N}{2}\right] \quad . \tag{32}$$

This starts small because for protons at room temperature in a 1T field the Boltzmann factor $\gamma\hbar B/kT \sim 10^{-6}$, and then decreases exponentially with N because of the partition function normalization of the thermal density matrix.

Fortunately, a number of old and new experimental techniques promise to bring this signal up to a useful level. Each increase of $10^3 \approx 2^{10}$ in signal strength adds enough sensitivity for roughly ten more bits. Because the magnetization is proportional to the field and inversely proportional to the temperature, linear improvements in these parameters do not contribute significantly. But since the electron gyromagnetic ratio is $\sim 10^3$ times larger than the nuclear gyromagnetic ratio, transferring its thermal polarization to the nuclear spins used in a computation leads to an increase in sensitivity by a factor of 10^3. This is analogous to cooling the spins' temperature by 10^3, and can be done by performing a controlled-NOT in the hyperfine-coupled electron-nucleus system. Another factor of 10^3 can come from transferring the result of a calculation back to the electronic system for readout, since for a given polarization the magnetization is proportional to the gyromagnetic ratio (electrons are less suitable for computation directly because of their sensitivity to environmental interactions).

NMR signals are usually detected inductively in a K turn pick-up coil with cross-sectional area A, in a resonant tank with a quality factor Q. The time-varying magnetization leads to a flux Φ in the coil which produces a peak-to-peak voltage

$$V = QK\frac{d\Phi}{dt} = QK\frac{d}{dt}\mu_0 M A \quad . \tag{33}$$

In the lab frame the readout magnetization will rotate at the Larmor frequency $\gamma_A B$, therefore the amplitude of the oscillating voltage in the pick-up coil will be

$$V = QK(\gamma_A B)\mu_0 \left[n\gamma_A \hbar \frac{1}{2^N} \frac{\gamma_B \hbar B}{kT} \frac{N}{2} \right] A . \qquad (34)$$

Because of the time derivative, moving the readout up to electron spin resonance frequencies gives another factor of 10^3 improvement in the voltage produced by a coil. Since the cross-sectional area is quadratic in the radius of the coil, increasing the sample radius by a factor of ~ 30 gives another factor of 10^3 (this is possible because unlike conventional analytical NMR a commodity liquid can be used). Furthermore, the Q of the pick-up tank is usually intentionally decreased to maintain sensitivity over the bandwidth of interest. Since the spectroscopy of the liquid used for computation is known in advance, a single line can be chosen for readout and a high-Q resonator can be tuned to it. This increases the signal proportional to the Q, leading to another factor conservatively of 10^2.

Taken together these relatively straightforward experimental modifications suggest that sensitivity for many tens of bits should be possible, bringing quantum computation up to a size that begins to surpass the size of the largest classical computers (a 40 qubit quantum computer has $2^{40} \sim 10^{12}$ classical degrees of freedom). To scale still further it will be necessary to make the spin polarizations on the order of unity; this occurs in systems that use optical pumping to drive hyperfine transitions, or cryogenic cooling to reach millikelvin temperatures.

As N is increased a second concern is the scaling of the time to apply gates. The effective clock cycle of an NMR computer is the spin precession period associated with the weakest interaction term used, which are the nonlinear exchange couplings. These typically range from milliseconds (kHz) to seconds (Hz). Because a quantum computer can do exponentially more work per cycle than a classical computer, even these slow rates are acceptable. The fastest classical factoring algorithm for arbitrary large integers is the Number Field Sieve [29], requiring

$$O\left(e^{1.923+(\log N)^{1/3}(\log\log N)^{2/3}}\right) \qquad (35)$$

operations to factor a number N. Ignoring prefactors (which can be large), factoring a 1000 digit number would require $O(10^{23})$ operations, which on a Gflop computer would take $O(10^7)$ years. Shor's quantum factoring algorithm requires

$$O((\log N)^{2+\epsilon}) \qquad (36)$$

steps, giving $O(10^6)$ operations for a 1000 digit number (again ignoring prefactors). If we assume a one Hertz gate time, that brings the time to factor 1000 digits down to just 11 days. This assumes that all the pairwise interaction terms can be directly resolved; as N is increased the interactions between distant spins will no longer be resolvable. Fortunately universal quantum computation is still feasible with just local interactions, by using a quantum cellular automata architecture that results in a linear increase in the computational time with system size due to message passing [8].

The final scaling issue is the coherence time. In liquid NMR, irreversible decoherence occurs on (T_1 and T_2) times that range from seconds to thousands of seconds. This gives $O(10^3)$ coherent operations within a coherence time, demonstrated by the longest pulse sequences used in multi-dimensional NMR spectroscopy. The inverse of this, 10^{-3}, approaches to within one or two orders of magnitude the coherence believed to be needed for steady-state quantum error correction [30,31] (at the expense of signal strength due to the addition of ancilla). Therefore, with error correction usefully long sequences should be possible.

Although these calculations are encouraging for the eventual scaling to non-trivial applications, our preliminary experiments to be described next have used small systems to address the fundamental issues of operating and characterizing a bulk quantum computer.

III. EXPERIMENTAL NMR RESULTS

Experiments were performed using nuclear magnetic resonance to test the ability to prepare elementary states, to implement a primitive quantum logic gate, to cascade gates to create simple circuits, and to create effective pure states. These experiments were performed using a molecule whose structure was already completely determined, allowing us to focus instead on the capacity of the system to perform quantum computations. We developed a technique to perform quantum state tomography, and applied it to test quantum state creation and transformation programs. These included single qubit rotations and a controlled-NOT gate, which form a universal set of operations [4]. We demonstrated these in action by implementing a quantum circuit to create a mixture of Einstein-Podolsky-Rosen (Bell) states [20]. Finally, we cascaded two controlled-NOT gates to implement a permutation gate, and created effective pure states using temporal labeling. These results are surveyed below; more detailed descriptions and analyses including larger systems will be presented elsewhere.

A. Apparatus and Molecule

The two-spin physical system used in these experiments was carbon-13 labeled chloroform (Fig. 3) supplied from Cambridge Isotope Laboratories, Inc. (catalog no. CLM-262), and was used without further purification. A 0.5 milliliter, 200 millimolar sample was prepared with d6-acetone as a solvent, degassed, and flame sealed in a thin walled, high performance 5mm NMR sample tube.

This sample was in liquid form, and experiments were performed at room temperature.
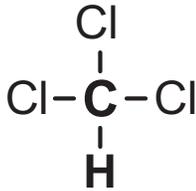
FIG. 3. Molecule of chloroform: the two active spins in this system are the ^{13}C and the ^{1}H.

The Hamiltonian for this system can be modeled as a two-spin system with a Zeeman interaction,

$$\hat{\mathcal{H}} = \omega_A \hat{I}_{zA} + \omega_B \hat{I}_{zB} + 2\omega_{AB} \hat{I}_{zA} \hat{I}_{zB} + \hat{\mathcal{H}}_{env} , \quad (37)$$

where $\hat{\mathcal{H}}_{env}$ represents a coupling to an external reservoir, and $\hat{I}_{zA} = \sigma_{zA}/2$ is the angular momentum operator in the $\hat{z}$ direction for spin A (the proton, in our convention here). The reservoir includes small interactions with other nuclei such as the chlorine, which do not play a major role in the dynamics. It also includes higher order terms in the spin-spin coupling, which can be disregarded in the first-order model; the spin interaction is dominated by through-bond coupling mediated by electrons, rather than by direct dipole-dipole interaction between the nuclei, and in the liquid at a high magnetic field the rapid molecular tumbling averages away all but the $\hat{I}_{zA} \hat{I}_{zB}$ J-coupling.

Spectra were taken using Bruker AMX-400 (Berkeley) and DRX-500 (Los Alamos) spectrometers using standard probes. The deuterium resonance in the solvent was used as a lock signal for the magnetic field. The resonance frequencies of the two proton lines (in the DRX-500) were measured to be at 500.133921 MHz and 500.134136 MHz, and the carbon lines were at 125.767534 MHz and 125.767749 MHz, with errors of ± 1 Hz. The RF excitation carrier (and probe) frequencies were set at the midpoints of these peaks, so that the chemical shift evolution could be neglected, leaving only the 215 Hz J-coupling between the two spins. The nuclear resonance lines from the solvent were at least a kHz away, and did not play any role in the experiment.
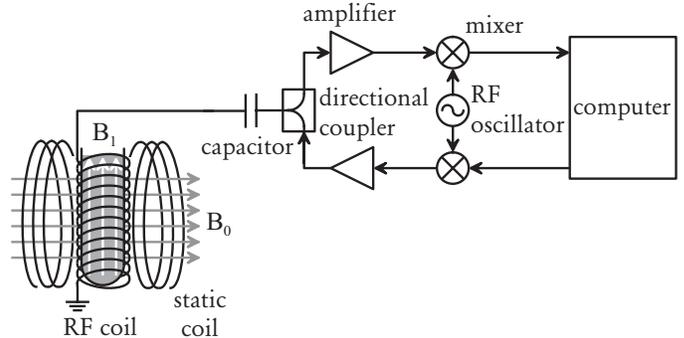
FIG. 4. (B) Schematic of an NMR apparatus.

A simplified schematic diagram of an NMR spectrometer appears in Fig. 4. The chloroform nuclei are perturbed by applying a much smaller radio-frequency (RF) field, B_1, in the transverse plane to excite the spins at their resonant frequencies ω_i. As described by the Bloch equations, these pulses can effect rotations of the nuclear moments about the $\hat{x}$ and $\hat{y}$ axes. For example, a 90° pulse can be applied to all the nuclei, to tip them from their equilibrium positions (aligned to B_0 along the $\hat{z}$ axis) into the transverse ($\hat{x}$-$\hat{y}$) plane, where their precession generates a small free induction decay signal which can be picked up by a phase sensitive detector coupled to the receiver coil.

The coherence times of the two spins were estimated by measuring T_1 and T_2 relaxation times, independently at both facilities on similarly prepared samples, using standard inversion-recovery and Carr-Purcell-Meiboom-Gill pulse sequences. For the proton, it was found that $T_1 \approx 7$ sec, and $T_2 \approx 2$ sec, and for carbon, $T_1 \approx 16$ sec, and $T_2 \approx 0.2$ sec. The short carbon T_2 time is due to coupling with the three quadrupolar chlorine nuclei, which reduces the coherence time.

B. Single spin operations

As already mentioned, applying RF pulses at the appropriate frequency and of the appropriate duration and amplitude allows any single spin rotation to be performed. In particular, we can apply pulses at either the proton or carbon frequencies, independently or simultaneously, and of arbitrary phase with reference to the carrier signal. It is sufficient to apply pulses around the $\hat{x}$ and $\hat{y}$ axes, because these generate all possible rotations on the Bloch sphere. We calibrated these pulses in the following manner. The data gathered by the spectrometer is the free induction decay signal, which gives

$$V(t) \approx \quad (38)$$
$$V_0 e^{-t/T_1} \mathrm{Tr}\left(e^{i\hat{\mathcal{H}}t}\hat{\rho}e^{-i\hat{\mathcal{H}}t}(i\hat{I}_{xA} + \hat{I}_{yA} + i\hat{I}_{xB} + \hat{I}_{yB})\right) .$$

Fourier transforming this signal gives a spectrum with four peaks, with Lorentzian lineshape. The areas of these peaks give four complex numbers which reflect the state of the system. As the length of a single applied RF pulse is varied, at fixed power, the (proton or carbon) peak areas change sinusoidally, giving a maximum for the "90 degree" pulse, and a null for a 180 degree pulse. These pulses flip the spin from the $\hat{z}$ axis into the $\hat{y}$ and $-\hat{z}$ directions, respectively, for a rotation phase around the $\hat{x}$ axis, and are described for example by $\hat{R}_x(\theta) = \exp(i\theta\sigma_x/2)$ operators (where σ_x is the usual Pauli matrix).

We tested this self-consistently, by using the calibrated pulses to measure components of the density matrix giving the state of the individual proton and carbon spins. For example, we measured the thermal state (deviation density matrix) of the proton to be

$$\hat{\rho}_a = \begin{bmatrix} 67 & -0.4 \\ -0.4 & -67 \end{bmatrix}, \qquad (39)$$

in arbitrary units. The result of an ideal rotation $\hat{R}_x(-\pi/2)$ would have been

$$\hat{\rho}'_a = \begin{bmatrix} -0.4 & 67i \\ -67i & -0.4 \end{bmatrix}, \qquad (40)$$

and the actual observed single-shot output was

$$\hat{\rho}'_a = \begin{bmatrix} 0.6 & 62i \\ -62i & -0.6 \end{bmatrix}. \qquad (41)$$

Detection noise contributed to the diagonals, which ideally should be zero. The decrease in the signal amplitude was primarily caused by magnetization decay (T_1 effects) during the acquisition of the free induction decay signal, and this was the primary source of overall error. Similar results were obtained for other pulse combinations, indicating single pulse rotation calibration to better than a few degrees.

C. State Tomography

A generalization of the measurement scheme used to calibrate single pulses allowed us to obtain all the elements in the two-spin density matrix. The basic procedure was to apply a sequence of RF pulses, measure the resulting induction signal, Fourier transform to get the spectra, and integrate to get the areas of the resonance peaks. The real and imaginary components of the area of each of the four peaks gave a total of eight numbers for each run. By applying different pulse sequences, all the elements in the 4×4 density matrix were sampled, allowing a least-squares procedure to recover $\hat{\rho}$ from the data.

Two different approaches were used in designing the pulse sequences: the simpler method involved performing nine runs, in which each nucleus was either left alone (I), tipped by 90° around the X axis, or around the Y axis. Explicitly, the nine pulse programs were II, IX, IY, XI, XX, XY, YI, YX, and YY. Of course, II gave no signal, but it provided a baseline for noise estimation. The second method involved more complicated pulse sequences and the use of phase cycling to create multiple quantum filters to improve the signal-to-noise ratio (to be published elsewhere).

The resulting experimentally measured deviation density matrix for the thermal state was approximately

$$\hat{\rho} \approx \begin{bmatrix} 48 & 0 & 0 & 0 \\ 0 & 28 & 0 & 0 \\ 0 & 0 & -28 & 0 \\ 0 & 0 & 0 & -48 \end{bmatrix}, \qquad (42)$$

(in arbitrary units; numbers of absolute value smaller than 0.8 suppressed for clarity), in the basis $|00\rangle$, $|01\rangle$, $|10\rangle$, and $|11\rangle$, from left to right. As expected, all the off-diagonal elements are nearly zero, while the diagonal elements follow a pattern of $a + b$, $a - b$, $-a + b$, and $-a - b$. The ratio $a/b = 3.98$ is fixed by the ratio of the gyromagnetic frequencies of the two nuclei, and was used to calibrate the relative strength of the carbon signal amplification and digitization circuitry to that of the proton. An error of about 5% was observed in the data, due primarily to imperfect calibration of the 90° pulse times and inhomogeneity of the magnetic field.

This diagonal matrix reflects a state which can be understood as a mixture of $|00\rangle$, $|01\rangle$, $|10\rangle$, and $|11\rangle$ states. In fact, as von Neumann pointed out, many pure state decompositions generally exist for a given mixed state density matrix, but as long as no further information is available about the ensemble, it is impossible to assign a reality to one particular decomposition: they are all equally real. This principle is important in the way we interpret our data.

D. Controlled-NOT Gate

The experimental configuration we used provided us with a simple means for implementing a controlled-NOT gate, which is shown in Fig. 5. The ideal transformation is

$$\hat{CN}_{ideal} = \begin{bmatrix} 1 & 0 & 0 & 0 \\ 0 & 1 & 0 & 0 \\ 0 & 0 & 0 & 1 \\ 0 & 0 & 1 & 0 \end{bmatrix}, \qquad (43)$$

which can be understood to invert spin b only when spin a is 1, and to do nothing if $a = 0$. Now, as previously mentioned, by putting the RF carriers on resonance with

the spin frequencies, the chemical shift evolution could be neglected; in other words, in the doubly rotating frame, ω_A and ω_B are both zero. Therefore, applying the pulse sequence in Fig. 5 gave us the unitary transform

$$\hat{CN}_{pp} = \begin{bmatrix} (-1)^{1/4} & 0 & 0 & 0 \\ 0 & -(-1)^{3/4} & 0 & 0 \\ 0 & 0 & 0 & (-1)^{1/4} \\ 0 & 0 & (-1)^{3/4} & 0 \end{bmatrix}, \tag{44}$$

which has a similar controlled-NOT effect as the ideal transform, and acts as expected on "classical" states such as $|00\rangle\langle00|$, $|01\rangle\langle01|$, $|10\rangle\langle10|$, and $|11\rangle\langle11|$. It differs in its relative phases, but that effect shows up only when operating on superposition states. A single controlled-NOT pulse program applied to the a thermal state gave us

$$\hat{CN}_{pp} \begin{bmatrix} 42 & 0 & 0 & 0 \\ 0 & 25 & 0 & 0 \\ 0 & 0 & -26 & 0 \\ 0 & 0 & 0 & -41 \end{bmatrix} \hat{CN}_{pp}^\dagger = \begin{bmatrix} 44 & 0 & 0 & 0 \\ 0 & 25 & 0 & 0 \\ 0 & 0 & -41 & 0 \\ 0 & 0 & 0 & -28 \end{bmatrix} \tag{45}$$

These data have an error of ± 3 units from being taken several hours apart, after the magnetic field had drifted slightly, but clearly show the expected transformation from the controlled-NOT operation. Other transform elements from the expected truth-table were also confirmed, and its proper operation on superposition states was systematically verified. An application which demonstrates this is presented next.
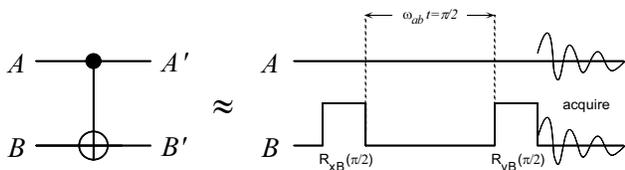
FIG. 5. Quantum circuit symbol for a controlled-NOT gate, and its implementation with RF pulses in our two-spin NMR system in the doubly degenerate frame. The time $\pi/2\omega_{AB}$ was 2.326 milliseconds in the experiment.

E. Einstein-Podolsky-Rosen State Mixtures

As an application of the controlled-NOT gate, we used it in a simple quantum circuit to create entangled states from the thermal mixture. The most important example of two-qubit entangled states are the Einstein-Podolsky-Rosen (EPR) states, shown in Eq. (48)-(51). A quantum circuit which creates EPR states from $|00\rangle$ is shown in

Fig. 6. The unitary transform implemented by the ideal circuit is

$$\hat{U}_{ideal} = \frac{1}{\sqrt{2}} \begin{bmatrix} 1 & 0 & 1 & 0 \\ 0 & 1 & 0 & 1 \\ 0 & -1 & 0 & 1 \\ -1 & 0 & 1 & 0 \end{bmatrix}, \tag{46}$$

while the actual transformation implemented by the pulse program was

$$\hat{U}_{pp} = \frac{1}{2} \begin{bmatrix} 1+i & 0 & -1+i & 0 \\ 0 & 1-i & 0 & 1+i \\ 0 & -1+i & 0 & 1+i \\ -1-i & 0 & -1+i & 0 \end{bmatrix}. \tag{47}$$

Although different, they served the same purpose: transforming each energy eigenstate into an EPR state. In particular,

$$|00\rangle \rightarrow |00\rangle - |11\rangle \tag{48}$$
$$|01\rangle \rightarrow |01\rangle - |10\rangle \tag{49}$$
$$|10\rangle \rightarrow |00\rangle + |11\rangle \tag{50}$$
$$|11\rangle \rightarrow |01\rangle + |10\rangle \tag{51}$$

(up to a normalization and phase) is accomplished by $\hat{U}_{pp}$. Note the different mapping which results from $\hat{U}_{pp}$ and $\hat{U}_{ideal}$ due to the phase differences between $\hat{CN}_{pp}$ and $\hat{CN}_{ideal}$. In the NMR literature, these states are known as *zero* and *double quantum coherence* states, and none of these states should give any output signal, as can be seen by calculating $V(t)$ using Eq. (38). This was observed, to within 5%.
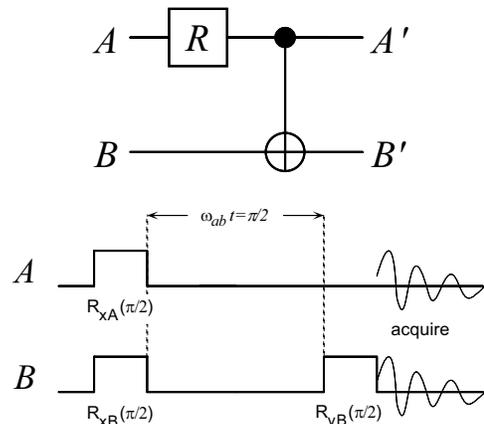
FIG. 6. (top) Quantum circuit, where the boxed R denotes the single-qubit rotation $\hat{R}_x(\pi/2)$, and (bottom) corresponding pulse program for creating an EPR state.

Complete characterization of this state was performed using state tomography. For the thermal deviation density matrix of Eq. (42) the expected result from the EPR procedure is

10

$$\hat{\rho}_{epr} = \hat{U}_{pp}\,\hat{\rho}\,\hat{U}_{pp}^{\dagger} = \frac{1}{4}\begin{bmatrix} 40 & 0 & 0 & -150 \\ 0 & -40 & -150 & 0 \\ 0 & -150 & -40 & 0 \\ -150 & 0 & 0 & 40 \end{bmatrix},$$
(52)

while the experimentally measured result was approximately

$$\frac{1}{4}\begin{bmatrix} 49 & 0 & 0 & -128 \\ 0 & -27 & -124 & 0 \\ 0 & -124 & -42 & 0 \\ -128 & 0 & 0 & 20 \end{bmatrix}.$$
(53)

The expected signs match exactly with the data, while the magnitudes of the reverse diagonal elements agree to within 20%. The element most different from that expected is the $|11\rangle\langle 11|$ entry, which deviates by 50%. Again, the primary cause of error was magnetization decay during the acquisition.

Perhaps the most interesting aspect of this experiment is that the experimental results cannot be explained by a classical model of two interacting spins (of spin 1/2). A classical spin is characterized by having a definite orientation in three dimensions. Let the interaction between two spins be such that the rate at which they spin around the $\hat{z}$ axis is proportional to the product of the $\hat{z}$ components of the two spins (fast if they are oppositely oriented, 01 or 10, slow if they point in the same direction, 00 or 11). This is analogous to the Hamiltonian describing the quantum system, Eq. (37). Now, what happens in the pulse sequence of Fig. 6 is that first the two spins are tipped into the transverse ($\hat{x} - \hat{y}$) plane, allowed to precess for a specific time, then one is tipped back up to the $\hat{z}$ axis. The other remains in the transverse plane. Classically, the spin in the $\hat{x} - \hat{y}$ plane will generate a signal $V(t)$ which should be detected by the receiver coil. Furthermore, if we rotate both spins around by 90°, then the other spin should generate a detectable signal.

However, this classically expected signal is not observed in practice. This is because the spins are actually quantum-mechanical – during their coupled evolution, they are in a superposition of being up and down, and therefore the coupled system evolves in a superposition of fast and slow states. They become entangled. When one spin is flipped back onto $\pm\hat{z}$, because of this entanglement, it turns out the other spin also gets flipped onto the $\hat{z}$ axis, and this happens in such a way that the two signals generated – from fast and slow states – *interfere* with each other and cancel out all detectable signals $V(t)$. This is true no matter how the system is rotated, as long as both spins are rotated in the same way. We have experimentally confirmed this behavior, and the signature of the entanglement – a purely *non-classical* effect – is the strong reverse diagonal measured in the density matrix.

F. Cascaded controlled-NOT Gates

An important challenge in creating a quantum computer is to cascade multiple logic gates together to build non-trivial quantum circuits. As a step in this direction, we cascaded two controlled-NOT gates together to implement a permutation operation, using the quantum circuit shown in Fig. 7. The ideal and actual transformations this accomplishes are

$$\hat{P}_{ideal} = \begin{bmatrix} 1 & 0 & 0 & 0 \\ 0 & 0 & 1 & 0 \\ 0 & 0 & 0 & 1 \\ 0 & 1 & 0 & 0 \end{bmatrix}$$
(54)

$$\hat{P}_{pp} = \begin{bmatrix} i & 0 & 0 & 0 \\ 0 & 0 & -1 & 0 \\ 0 & 0 & 0 & 1 \\ 0 & i & 0 & 0 \end{bmatrix}.$$

Applying this to a thermal input state gave us the experimental result

$$\hat{P}_{pp}\begin{bmatrix} 49 & 0 & 0 & 0 \\ 0 & 28 & 0 & 0 \\ 0 & 0 & -29 & 0 \\ 0 & 0 & 0 & -48 \end{bmatrix}\hat{P}_{pp}^{\dagger}$$
(55)

$$= \begin{bmatrix} 47 & 0 & 0 & 0 \\ 0 & -21 & 0 & 0 \\ 0 & 0 & -45 & 0 \\ 0 & 0 & 0 & 19 \end{bmatrix},$$

which agrees with the theoretically expected result, within the error margins of the experiment. This elementary two controlled-NOT circuit was useful for creating effective pure states, as described next.
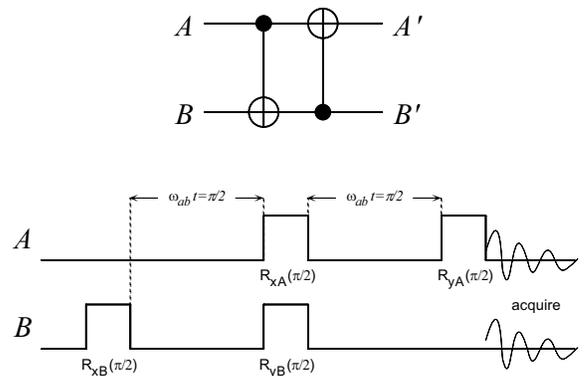
FIG. 7. Quantum circuit to perform a permutation operation, and its pulse program implementation.

G. Effective Pure State

An effective pure state of two qubits can be created using temporal labeling in the following way: three exper-

11

iments are performed, in each of which the computation $\mathcal{C}$ is preceded by a different preparation step P_i, where

$$\hat{P}_0 = \begin{bmatrix} 1 & 0 & 0 & 0 \\ 0 & 1 & 0 & 0 \\ 0 & 0 & 1 & 0 \\ 0 & 0 & 0 & 1 \end{bmatrix} \tag{56}$$

$$\hat{P}_1 = \begin{bmatrix} 1 & 0 & 0 & 0 \\ 0 & 0 & 1 & 0 \\ 0 & 0 & 0 & 1 \\ 0 & 1 & 0 & 0 \end{bmatrix} \tag{57}$$

$$\hat{P}_2 = \begin{bmatrix} 1 & 0 & 0 & 0 \\ 0 & 0 & 0 & 1 \\ 0 & 1 & 0 & 0 \\ 0 & 0 & 1 & 0 \end{bmatrix} . \tag{58}$$

$\hat{P}_0$ is the identity, and $\hat{P}_1$ and $\hat{P}_2$ are cyclic permutations of the three lower elements on the diagonal of the density matrix. For $\mathcal{C} = \mathcal{I}$ (no computation), and for any given input state, the output state will be of the form $\hat{\rho}_\epsilon = \mathrm{diag}(\alpha, -\delta, -\delta, -\delta)$, which is an effective pure state corresponding to $|00\rangle\langle 00|$.

These permutations are implemented simply using cascaded controlled-NOT gates, as previously described. Results from this experiment, shown in Fig. 8, show the expected "soloist" and "chorus" states. A detailed analysis of the quality of this experimental result is presented in [28].
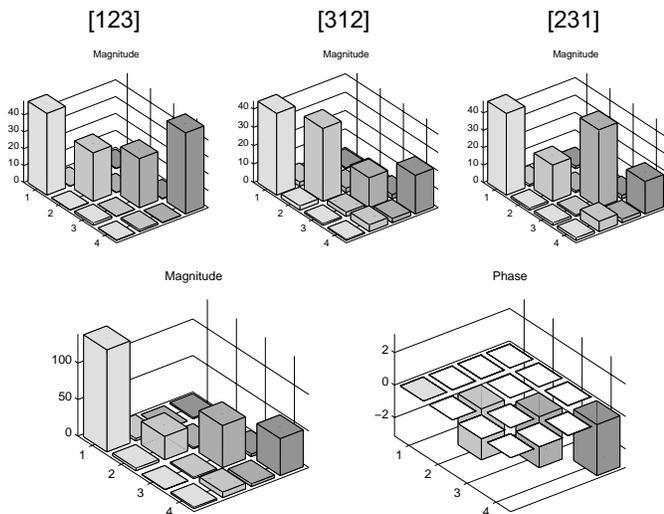
FIG. 8. (top) Three states which were summed to produce (bottom) an effective pure state.

H. Effectively Pure EPR State

Finally, we repeated our experiment to create EPR (Bell) states, using an effective pure state as an input. This circuit involved cascading *three* controlled-NOT

gates together in a non-trivial way to allow us to filter out the signal from just one of the four Bell states of Eqs. (48)-(51). This procedure is much the same as in the creation of the effective pure state above, but with $\mathcal{C}$ being the quantum circuit of Fig. 6 for creating an EPR state. This is theoretically described by the transformation

$$\hat{\rho}_{\mathrm{EPR}} = \sum_{k=0}^{2} \hat{U}_{pp} \hat{P}_k \, \hat{\rho}_{\mathrm{thermal}} \, \hat{P}_k^\dagger \hat{U}_{pp}^\dagger , \tag{59}$$

using Eqs. (56)-(58), and Eq. (47), and an output density matrix is predicted which has the structure

$$\hat{\rho}_{\mathrm{EPR}} = \alpha \begin{bmatrix} 1 & 0 & 0 & -1 \\ 0 & 0 & 0 & 0 \\ 0 & 0 & 0 & 0 \\ -1 & 0 & 0 & 1 \end{bmatrix} - \frac{\alpha}{2}\hat{I} , \tag{60}$$

which is the signature of the Bell state $|00\rangle - |11\rangle$. Experimentally, we measured the deviation density matrix

$$\begin{bmatrix} 65.3 & \epsilon & \epsilon & -74.0 \\ \epsilon & \epsilon & \epsilon & \epsilon \\ \epsilon & \epsilon & \epsilon & \epsilon \\ -74.0 & \epsilon & \epsilon & 58.6 \end{bmatrix} , \tag{61}$$

where $|\epsilon| < 11.6$. Again, errors were primarily due to magnetic field inhomogeneity and signal decay during a long acquisition period (of about 6 seconds). This result provides an early demonstration of the viability of using labeling techniques to create effective pure states for bulk spin quantum computation.

IV. CONCLUSION

These simple results demonstrate for the first time quantum logic gates cascaded into useful quantum circuits operating on pure states, with a complete experimental characterization of the state of the system. Familiar NMR spectroscopy techniques were used in an unfamiliar domain, bringing together the physics and chemistry of computation. Future experiments will address the reduction of noise and errors, and the scaling up to larger systems.

The implementation of cascaded controlled-NOT gates and effective pure states opens the way for exploration of larger bulk spin systems for quantum computation. Our realization of quantum state tomography is also a first step towards doing full quantum *process* tomography [32,33] to systematically measure the general quantum operation (*i.e.*, the superoperator) describing the decoherence mechanisms at work in the system.

Theoretically, the coming challenge will be to provide efficient implementations of state labeling for bulk quantum computation that take best advantage of logical,

spatial, and temporal labeling. State labeling techniques also introduce the idea of transforming a given unitary quantum computation into a new *robust* quantum computation which can act on mixed state inputs instead of just pure states, a technique which will be valuable to bulk quantum computation realizations other than NMR.

While daunting experimental challenges remain before bulk spin resonance quantum computation can begin to compete with classical computers, the rapid experimental progress following its recent introduction, and the encouraging scaling properties of this system, suggest that it may grow to become much more than a laboratory curiosity.

V. ACKNOWLEDGEMENTS

[19] N. Gershenfeld and I. L. Chuang, Science **275**, 350 (1997).
[20] A. Einstein, B. Podolsky, and N. Rosen, Phys. Rev. **47**, 777 (1935).
[21] B. W. Schumacher, Phys. Rev. A **54**, 2614 (1996).
[22] K. Kraus, Annals of Physics **64**, 311 (1970).
[23] D. Suter, K. T. Mueller, and A. Pines, Phys. Rev. Lett. **60**, 1218 (1988).
[24] D. Suter, A. Pines, and M. Mehring, Phys. Rev. Lett. **57**, 242 (1986).
[25] D. Cory, A. Fahmy, and T. Havel, Proc. Nat. Acad. Sci. **94**, 1634 (1997).
[26] E. Knill, 1997, personal communication.
[27] P. Shor, Polynomial-time algorithms for prime factorization and discrete logarithms on a quantum computer, 1997, to appear.
[28] E. Knill, R. Laflamme, and I. L. Chuang, Effective Pure States for Bulk Quantum Computation, 1997, in preparation.
[29] A. Lenstra and H. Lenstra, *The Development Of The Number Field Sieve*, Vol. 1554 of *Lecture notes in mathematics* (Springer-Verlag, New York, 1993).
[30] R. Laflamme and E. Knill, Submitted to Proc. Royal Soc. London A (1997).
[31] J. Preskill, Submitted to Proc. Royal Soc. London A (1997).
[32] I. L. Chuang and M. A. Nielsen, Prescription for experimental determination of the dynamics of a quantum black box, 1996, LANL E-print quant-ph/9610001.
[33] J. F. Poyatos, J. I. Cirac, and P. Zoller, Phys. Rev. Lett. **78**, 390 (1997).

[1] S. Lloyd, J. Mod. Opt. **41**, 2503 (1994).
[2] W. G. Unruh, Phys. Rev. A **51**, 992 (1995).
[3] I. L. Chuang, R. Laflamme, P. Shor, and W. H. Zurek, Science **270**, 1633 (1995).
[4] A. Barenco *et al.*, Phys. Rev. A **52**, 3457 (1995).
[5] M. B. Plenio and P. L. Knight, Phys. Rev. A **53**, 2986 (1996).
[6] R. Landauer, Phil. Trans. Roy. Soc. **A 353**, 367 (1995).
[7] R. Feynman, Found. Phys. **16**, 507 (1986).
[8] S. Lloyd, Science **261**, 1569 (1993).
[9] S. Bandyopadhyay and V. Roychowdhury, Jap. J. App. Phys **35**, 3350 (96).
[10] D. P. DiVincenzo, Phys. Rev. A **50**, 1015 (1995).
[11] J. Cirac and P. Zoller, Phys. Rev. Lett. **74**, 4091 (1995).
[12] I. L. Chuang and Y. Yamamoto, Phys. Rev. A **52**, 3489 (1995).
[13] Q. A. Turchette *et al.*, Phys. Rev. Lett. **75**, 4710 (1995).
[14] P. Domokos, J. Raimond, M. Brune, and S. Haroche, Phys. Rev. Lett. **52**, 3554 (1995).
[15] T. Sleator and H. Weinfurter, Phys. Rev. Lett. **74**, 4087 (1995).
[16] D. P. Divincenzo, Science **270**, 255 (1995).
[17] R. R. Ernst, G. Bodenhausen, and A. Wokaun, *Principles of Nuclear Magnetic Resonance in One and Two Dimensions* (Oxford University Press, Oxford, 1994).
[18] K. Wago *et al.*, J. Vac. Sci. B **14**, 1197 (1996).